DALTON
FULL PAPER

Structure and dynamics in metal phosphine complexes using advanced NMR studies with *para*-hydrogen induced polarisation

Barbara A. Messerle,*[a] Christopher J. Sleigh,[b] Martin G. Partridge[b] and Simon B. Duckett[b]

[a] *School of Chemistry, University of Sydney, Sydney, NSW 2006, Australia. E-mail: b.messerle@chem.usyd.edu.au*
[b] *Department of Chemistry, University of York, Heslington, York, UK YO10 5DD*

Received 22nd December 1998, Accepted 25th February 1999

The iridium and rhodium phosphine complexes $IrCl(CO)(PPh_3)_2$ **1** (Vaska's complex), $Rh(PMe_3)_4Cl$ **2**, and $Rh(PMe_3)_3Cl$ **3**, add H_2 to form the corresponding dihydrides. Exchange with *para*-hydrogen (*p*-H_2) provides a means of observing ^1H NMR signals due to the metal bound hydrides at significantly enhanced levels of sensitivity. We show that monitoring these metal hydride complexes can be achieved by a range of 2D NMR methods, based on standard experiments, which have been modified to achieve optimum signal. The assignment of heteronuclei, including low sensitivity nuclei such as ^{103}Rh, determination of heteronuclear coupling constants and measurement of their relative signs, is described for these systems using *p*-H_2 derived starting magnetisation. In the case of Vaska's complex the dihydride addition product contains a *trans* labilised carbonyl ligand, and substitution with appropriate phosphines brings about the formation of metal phosphine complexes with new ligand spheres. Appropriately modified NOESY experiments are demonstrated to rapidly probe structural arrangements, and monitor dihydride exchange. For $Ir(H)_2Cl(PPh_3)_3$ dihydride exchange is shown to proceed mainly *via* $Ir(H)_2Cl(PPh_3)_2$, which is shown to contain inequivalent hydrides. The reactivity of the arsine complex $IrCl(AsPh_3)_3$ **9** towards H_2 is examined, and the NOESY approach used to make structural assignments in the reaction product.

Introduction

The elucidation of the structure of reaction products, and intermediates, is always central to understanding the way in which a catalyst functions. Nuclear magnetic resonance (NMR) provides a way to do this in solution using the same conditions of temperature and concentration that are normally found when a catalyst is used in anger. However, intrinsic limitations arise in the area of sensitivity associated with NMR spectroscopy due to the relatively small Boltzmann excess of magnetically active nuclei that are available for detection. Not surprisingly, examining the relatively sensitive proton nucleus has proved to be an essential feature of NMR because of its prevalence in chemical systems. The addition of protons, as dihydrogen, to metal complexes represents a key reaction in inorganic chemistry because of its central role in hydrogenation and hydroformylation catalysis. Unfortunately, catalytically significant species are normally present at such low concentrations that they are not normally observable by NMR. However, the size of the detectable NMR signal can be readily enhanced by utilising non-Boltzmann populations.[1]

The *para*-hydrogen (*p*-H_2) effect represents one efficient way of achieving enhancement using non-Boltzmann populations. This approach makes use of the fact that molecular hydrogen, H_2, exists in two quantum states, *ortho*-hydrogen, *o*-H_2, and *para*-hydrogen, *p*-H_2. Significantly, because the *para* isomer is restricted to even rotational states, it can be readily formed in concentrations that are much higher than the usual Boltzmann population excesses utilised in standard NMR methods. Transport of the two protons of *p*-H_2 into new magnetically inequivalent environments yields products in which the spin populations of the transferred protons initially reflect those of the starting dihydrogen when spin correlation is maintained during addition. Since the success of this approach was first predicted,[2] large enhancements of NMR signal intensity have been reported in NMR spectra of product nuclei that arise from those of *p*-H_2, or possess a direct scalar coupling to these nuclei. This enhancement phenomenon has been termed PASADENA by Weitekamp[3] and *para*-hydrogen induced polarisation (PHIP) by Eisenberg.[4]

H_2 transfer processes occur readily in catalytic hydrogenation reactions and large NMR signal enhancements often result with *p*-H_2.[5] The requirement that PHIP is observed only when hydrogen transfer occurs in a concerted manner also means that the observation of PHIP is definitive evidence for pairwise hydrogen transfer.[6] In addition, the significant signal enhancement achieved by PHIP has made it possible to observe inorganic species that are present in such low concentrations that they are not normally visible.[7] For example, the direct observation *via* PHIP of products resulting from H_2 oxidative addition to Wilkinson's complex $RhCl(PPh_3)_3$, such as $Rh(H)_2Cl(alkene)(PPh_3)_2$, has led to important conclusions about the reaction mechanism of hydrogenation using Wilkinson's complex.[8]

In order to capitalise on the potential signal enhancement provided by *p*-H_2, the magnetisation from the *p*-H_2 signal must be actively transferred to other magnetically active, coupled, nuclei. The 1D INEPT sequence has been used extensively with *p*-H_2 to transfer polarisation from protons to heteronuclei in order to aid their detection.[9] Other approaches have been the subject of a recent review.[10]

Here we show that metal dihydride addition products can be rapidly monitored by a range of high sensitivity 2D NMR methods which differ from their standard counterparts in as far as they have been modified to achieve optimum signal with *p*-H_2.[11] We illustrate this by referring to specific examples taken from metal phosphine chemistry. The iridium and rhodium complexes, $IrCl(CO)(PPh_3)_2$ **1** (Vaska's complex), $Rh(PMe_3)_4Cl$ **2**, and $RhCl(PMe_3)_3$ **3**, were selected because they add H_2 to form the simple dihydride adducts, $IrH_2Cl(CO)(PPh_3)_2$ **4**, $[RhH_2(PMe_3)_4]Cl$ **5**, and $RhH_2Cl(PMe_3)_3$ **6**, respectively. In Vaska's complex, the dihydride product contains a *trans* labilised carbonyl ligand, and substitution with appropriate phosphines brings about the formation of metal phosphine complexes with new ligand spheres.[12] The closely related complex $IrH_2Cl(AsPh_3)_3$ **10** was also examined. In the case of **2** and

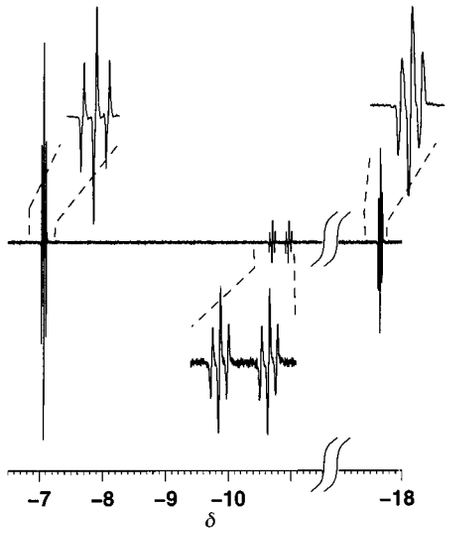

Fig. 1 ^{1}H NMR spectrum collected with a π/4 pulse, showing *para*-hydrogen enhanced hydride resonances for $IrH_2Cl(CO)(PPh_3)_2$ **4**, and $IrH_2Cl(PPh_3)_3$ **7**.

3, the NMR methods allow the observation of heteronuclear chemical shift information for low sensitivity nuclei such as ^{103}Rh, the determination of heteronuclear coupling constants and measurement of their relative signs.[13] Appropriately modified NOESY experiments were used to rapidly probe product ligand arrangements and investigate dihydride exchange processes. The methodologies illustrated here are appropriate for the examination of the ligand sphere of any *p*-H_2 enhanced product. Some of this work has been featured in preliminary communications.[12,13]

Results and discussion

The time averaged spin state of the starting hydride magnetisation in a *p*-H_2 derived dihydride is longitudinal two spin order, and can be represented by the product operator formalism[14] as $I_{AZ}I_{BZ}$ where A and B represent the two protons that originated from *p*-H_2.[15] On application of a hard pulse of flip angle φ about the *x* axis, the magnetisation becomes: $\frac{1}{2}\{I_{AZ}I_{BZ}\cos2\varphi - I_{AZ}I_{BY}\sin2\varphi - I_{AY}I_{BZ}\sin2\varphi + I_{AY}I_{BY}\sin2\varphi\}$ and the observable signal arises from the anti-phase I_ZI_Y terms. When A and B represent inequivalent hydride ligands, the resonances for A and B appear anti-phase with respect to *J*(AB), the coupling constant between the two hydrogen nuclei, and yield optimal signal intensity when φ is π/4 (this effect is illustrated in Fig. 1). The anti-phase magnetisation generated by application of π/4 pulse will follow the usual evolution pathways. Appropriate pulse sequences can therefore be used, or modified, to establish through bond and through space connectivity within molecules containing *p*-H_2 enhanced spins.

When a 1 mM solution of **1** in d_8-toluene under 3 atm of *p*-H_2 is warmed to 343 K and monitored by ^{1}H NMR spectroscopy, enhanced resonances are detected for the hydride ligands of $IrH_2Cl(CO)(PPh_3)_2$ **4**. The observation of *p*-H_2 enhanced hydride resonances at δ −7.02 and −17.6 confirms that hydrogen addition proceeds *via* a concerted pathway. The relative sign of the antiphase signal observed for a *p*-H_2 enhanced signal (*i.e.* emission/absorption or absorption/emission) gives the relative sign of the H–H coupling, which in turn provides information about the relative disposition of the coupled hydrides. In the case of **4**, the emission/absorption character of each of the two hydride resonances confirms that *J*(HH) is negative (Fig. 1), and the two metal bound hydrides are *cis*. When this process is repeated with a 45-fold excess of PPh_3 relative to **1**, enhanced resonances are detected for the hydride ligands of $IrH_2Cl(PPh_3)_3$ **7** in addition to those of $IrH_2Cl(CO)(PPh_3)_2$ **4** (Scheme 1). The observed resonance

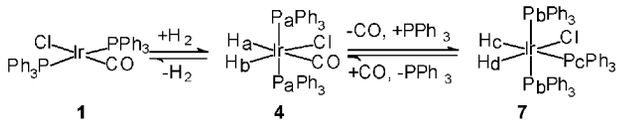

Scheme 1

positions, and multiplicities, match those previously attributed to these products.[16,12]

In a similar way, the addition of *p*-H_2 to CD_2Cl_2 solutions of $[Rh(PMe_3)_4]Cl$ **2**, and $RhCl(PMe_3)_3$ **3**, yields *p*-H_2 enhanced hydride resonances for $[RhH_2(PMe_3)_4]Cl$ **5**, and $RhH_2Cl(PMe_3)_3$ **6**, respectively.[17,18] With **2**, in addition to the polarised hydride resonances corresponding to **5**, signals for the monohydride complex $RhHCl_2(PMe_3)_3$ **8**, were observed and this product eventually becomes the dominant species in solution.[19] Similar results were obtained when samples of **3** and *p*-H_2 were warmed to 325 K, where polarised hydride resonances corresponding to those of **6** were observed initially, with the monohydride complex **8** again eventually becoming the dominant species in solution. Scheme 2 summarises the equilibria that are present in these solutions.

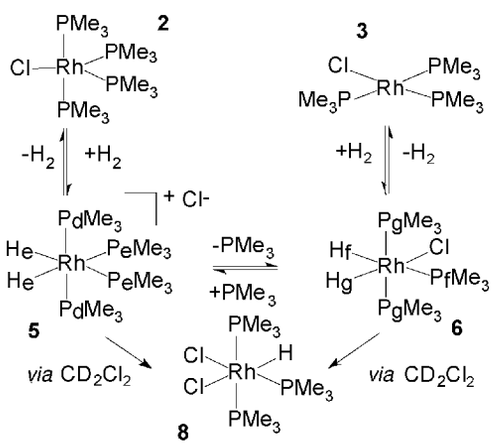

Scheme 2

Connectivity and coupling constants

For systems containing several dihydride complexes the rapid determination of hydride connectivity becomes vital. In order to determine H–H connectivity between the enhanced hydride resonances in the simple model systems under investigation here a minimally modified COSY experiment was used.[20] Simply replacing the first pulse (π/2) of a COSY experiment with a π/4 pulse enables *p*-H_2 enhanced COSY spectra to be acquired (Fig. 2a). The COSY experiment was used rather than the DQ-COSY experiment because of the higher sensitivity of the COSY experiment, and the fact that the diagonal peaks do not have significant intensity in these experiments. This arises due to the fact that in a COSY experiment, optimum signal transfer, and hence cross-peak formation, occurs when the transverse magnetisation evolving during t_1 is anti-phase with respect to the coupling allowing the correlation. Thus the anti-phase magnetisation created by the initial π/4 pulse in a *p*-H_2 experiment is already in the optimum state for signal transfer between the coupled pairs of hydride protons. At the onset of the experiment, the intensity of the COSY cross-peaks connecting enhanced proton pairs far outweighs those of their diagonal counterparts. Coupled pairs of *p*-H_2 enhanced hydrides can therefore be assigned quickly, and consequently relatively few increments are required to obtain useful spectra. In the case of the spectra collected on the Vaska's based system (Scheme 1), the connectivity of the hydride pairs due to **4** and **7** was easily confirmed using the modified COSY sequence (Fig. 3). As predicted, the intensity of the cross-peaks connecting H_a and H_b

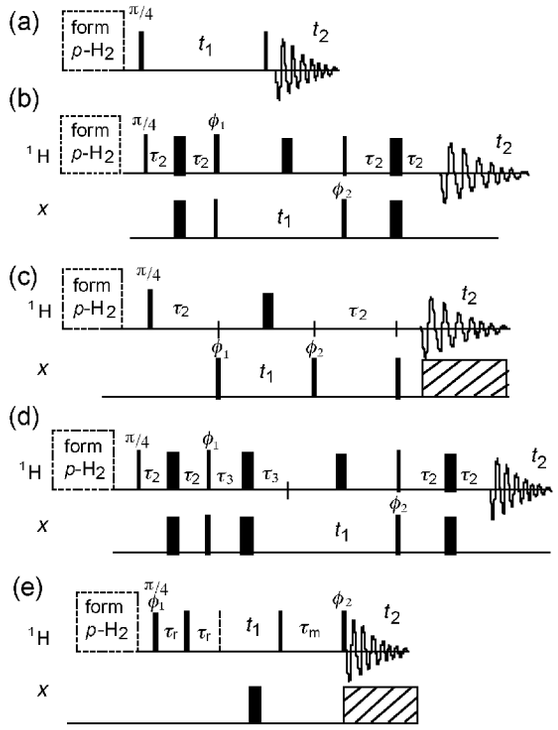

Fig. 2 Pulse sequences modified to allow magnetisation transfer from p-H_2 enhanced signal: (a) COSY (standard COSY phase cycling was used); (b) HSQC: $\varphi_1 = x,-x$, $\varphi_2 = x, x,-x,-x$, receiver $= x,-x,-x, x$; (c) HMQC: $\varphi_1 = x,-x$, $\varphi_2 = x, x,-x,-x$, receiver $x,-x,-x, x$; (d) H–X–H relay $\varphi_1 = x,-x$, $\varphi_2 = x, x,-x,-x$, receiver $x,-x,-x, x$; (e) NOESY with heteronuclear decoupling: $\varphi_1 = x,-x$, $\varphi_2 = x, x, -x, -x, y, y, -y,-y$ receiver $= x, -x, -x, x, y, -y,-y, y$. The dashed boxes indicate composite pulse decoupling, t_1 was used as the incremental delay defining F1, the thin lines indicate π/2 pulses unless otherwise shown and the thicker lines indicate π pulses.

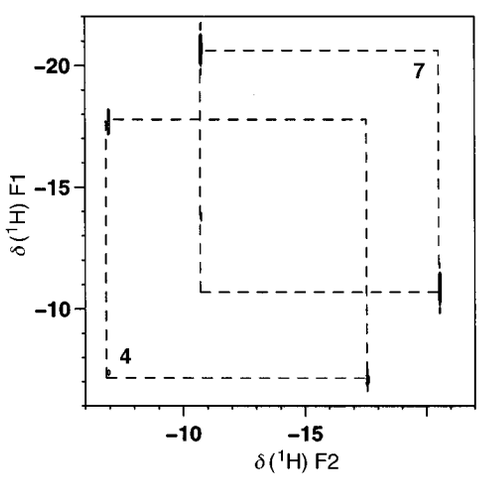

Fig. 3 Selected cross-peaks and projections from COSY spectra obtained using the sequence given in Fig. 2a for $IrH_2Cl(CO)(PPh_3)_2$ **4**, and $IrH_2Cl(PPh_3)_3$ **7** (complexes generated by warming **1** with a 45-fold excess of PPh_3 in C_6D_6 under p-H_2, 343 K). Experimental parameters: t_{1max} = 39.5 ms, t_{2max} = 99.8 ms, experimental time = 2.6 min.

in **4**, and H_c and H_d in **7** far exceeds that of their diagonal counterparts.

In order to assign heteronuclear spins which are coupled to p-H_2 enhanced proton magnetisation, modified 2D heteronuclear correlation experiments were employed. Both the heteronuclear single quantum correlation (HSQC)[21,22] pulse sequence and the heteronuclear multiple quantum correlation pulse sequence (HMQC)[23] were used to obtain 2D heteronuclear correlation spectra which employ the sensitivity of the p-H_2 enhancement. On application of an initial pulse of length

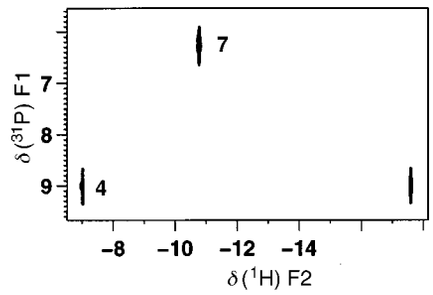

Fig. 4 HSQC showing connectivity between ^1H and ^{31}P resonances for the mixture of $IrH_2Cl(CO)(PPh_3)_2$ **4**, and $IrH_2Cl(PPh_3)_3$, **7**, formed on addition of p-H_2 to **1**. Experimental parameters: τ_2 = 7.0 ms, t_{1max} = 12 ms, t_{2max} = 44 ms, experimental time = 5 min.

π/4 to pairs of protons derived from p-H_2, the magnetisation generated is anti-phase with respect to proton couplings only, as described by the terms $I_{AZ}I_{BY}$ and $I_{BZ}I_{AY}$. In order to achieve magnetisation transfer to coupled heteronuclear spins, the proton magnetisation must evolve with respect to heteronuclear couplings prior to the pulses which achieve magnetisation transfer to heteronuclei. In both the HSQC and HMQC experiments (Fig. 2b and 2c), the proton spins evolve with both J(HH) and J(HX) during τ_2. In organometallic complexes J(HH) is typically small, corresponding to a slow evolution time, and consequently it was only necessary to modify the HSQC and HMQC experiments by replacing the initial π/2 pulse to protons with a π/4 pulse (Fig. 2b and 2c). The fixed delays (τ_2, Fig. 2b and 2c) were then optimised for heteronuclear magnetisation transfer. The HMQC sequence was completed with a purge pulse.

In a typical ^1H–^{31}P HSQC spectrum, cross-peaks connecting the resonances of the phosphorus nuclei to the resonances of their hydride coupling partners are visible. This approach therefore allows the assignment of ^{31}P chemical shift information in samples containing several p-H_2 enhanced products. In the ^1H–^{31}P HSQC spectra, the relative intensities of the cross-peaks depend on the value of τ_2. The spectrum shown in Fig. 4 corresponds to a typical HSQC spectrum obtained for the mixture of **4** and **7**, and allows assignment of the phosphorus nuclei in each hydride species. The delay τ_2 was set such that correlations to ^{31}P for both H_a and H_b of **4** were observed, and correlation to ^{31}P of only H_c of **7** was observed (Fig. 4).

In the case of the rhodium complexes $[Rh(PMe_3)_4]Cl$ **2**, and $RhCl(PMe_3)_3$ **3**, the ^{31}P resonances due to the corresponding H_2 addition products $[RhH_2(PMe_3)_4]Cl$ **5**, and $RhH_2Cl(PMe_3)_3$ **6**, were assigned using a modified HMQC experiment (Fig. 2c). The spectra (Fig. 5a–5d) were collected on samples of **2** and **3** which were warmed under p-H_2 in CD_2Cl_2 solution. Again in the ^1H–^{31}P HMQC spectra, the relative intensities of the cross-peaks depend on the value of τ_2. In the case of the p-H_2 enhanced product **6**, when the value of τ_2 is set to $\frac{1}{2}J(P_fH_f)$ the strongest cross-peak connects the hydride resonance at $\delta(^1H)$ −9.79 due to H_f to the phosphorus resonance at $\delta(^{31}P)$ −21.3 (Fig. 5a). On acquiring a ^1H–^{31}P HMQC experiment with the delay τ_2 set to $\frac{1}{2}J(P_gH_g)$ the observed cross-peak connects signals due to H_g at $\delta(^1H)$ −19.5 to the resonance for P_g at $\delta(^{31}P)$ −7.4 (Fig. 5b). Although the short data storage time of 25–250 ms used in the recording of these HMQC experiments precluded the observation of the H_f–H_g coupling [J(HH) = −8 Hz], it was sufficient to allow the observation of the larger rhodium-hydrogen couplings as indicated in the figures.

The related complex $[RhH_2(PMe_3)_4]Cl$ **5**, illustrates that p-H_2 enhanced resonances can also be observed when two chemically equivalent, but magnetically inequivalent hydride ligands are present. In the fully coupled ^1H–^{31}P HMQC experiment (Fig. 5c), the ^{31}P resonance for nucleus P_d shows passive couplings to rhodium and phosphorus (multiplet selection causes the loss of the central triplet feature) with J(RhP) = 96 Hz and J(PP) = 28

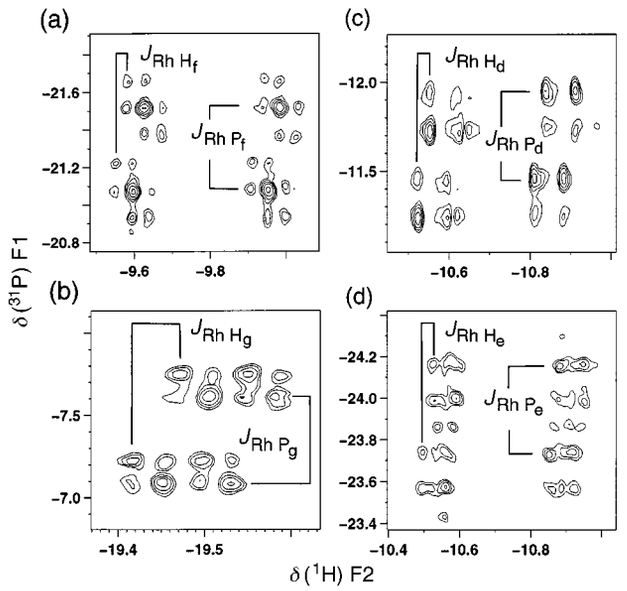

Fig. 5 HMQC spectra acquired using the sequence given in Fig. 2c, showing the connectivity between ^{1}H and ^{31}P resonances due to $[RhH_2(PMe_3)_4]Cl$ **5**, and $RhH_2Cl(PMe_3)_3$ **6**, formed on addition of *p*-H_2 to **2** and **3** respectively in CD_2Cl_2. Cross-peaks due to (a) P_fH_f of **6**. Experimental parameters: $\tau_2 = 3$ms, $t_{1max} = 39.5$ ms, $t_{2max} = 100.0$ ms, experimental time = 5.8 min. (b) P_gH_g of **6**. Experimental parameters: $\tau_2 = 12.5$ ms, $t_{1max} = 24.5$ ms, $t_{2max} = 100.0$ ms, experimental time = 5.1 mins. (c) HP_d of **5**. Experimental parameters: $\tau_2 = 3.7$ ms, $t_{1max} = 63.2$ ms, $t_{2max} = 100.0$ ms, experimental time = 16 min. (d) HP_e of **5**. Experimental parameters: $\tau_2 = 5.6$ ms, $t_{1max} = 31.6$ ms, $t_{2max} = 100.0$ ms, experimental time = 9.2 min. (No decoupling of ^{31}P was used in F2 for these experiments.)

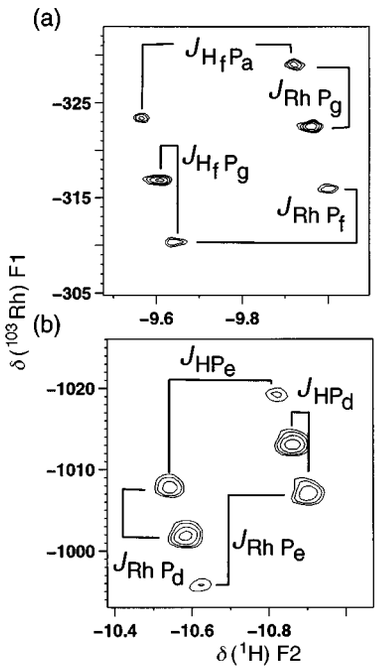

Fig. 6 (a) ^{1}H–^{103}Rh correlation spectrum (HMQC), ^{103}Rh decoupled in F2, acquired using $\tau = \frac{1}{2}J(RhH_f)$ for multiplet selection, showing correlated transitions between H_f and ^{103}Rh in **6**. Experimental parameters: $\tau_2 = 16.7$ ms, $t_{1max} = 67.5$ ms, $t_{2max} = 74.6$ ms, experimental time = 3.8 min. (b) ^{1}H–^{103}Rh correlation spectrum (HMQC), ^{103}Rh decoupled in F2, showing correlation between resonances due to ^{1}H and ^{103}Rh in **5**. Experimental parameters: $\tau_2 = 30.5$ ms, $t_{1max} = 20.3$ ms, $t_{2max} = 19.6$ ms, experimental time = 3.0 min.

Hz. The higher field phosphine signal due to P_e (Fig. 5d) appears as a complex multiplet from which J(RhP) = 86 Hz can be extracted.

The resonances due to the ^{103}Rh nuclei of the H_2 addition products of **2** and **3** were also observed *via* their most sensitive *p*-H_2 enhanced ^{1}H signature (Fig. 6). In the ^{1}H–^{103}Rh correlation spectrum of **6**, acquired with rhodium decoupling during acquisition (Fig. 6a), the hydride at $\delta(^1H)$ −9.79 is correlated to the rhodium centre at $\delta(^{103}Rh)$ −319. The corresponding ^{1}H–^{103}Rh correlation spectrum of **5** acquired with rhodium decoupling shows that the hydride at $\delta(^1H)$ −10.72 is coupled to the rhodium centre at $\delta(^{103}Rh)$ −1007 (Fig. 6b).

Heteronuclear coupling constants

The measurement of coupling constants is an essential part of the characterisation of the structure of organic and organometallic compounds by NMR spectroscopy. Both homonuclear and heteronuclear coupling constants are sensitive to the electronic structure of bonded atoms and molecular geometry in terms of dihedral angles.[24] In organometallic compounds, the magnitude of homo- and hetero-nuclear coupling constants can provide information about the stereochemistry of metal complexes as well as the oxidation state and co-ordination geometry of the central metal atom.[25] A number of NMR techniques are available to facilitate the measurement of coupling constants, including homonuclear 2D experiments such as ECOSY,[26] selective excitation methods,[27] and heteronuclear 2D experiments.[28]

The magnitude of the heteronuclear coupling constants were measured *via* passive couplings in the heteronuclear correlation spectra of compounds **5** and **6** presented in Figs. 5 and 6. The spectra presented are those acquired with decoupling, *i.e.* the active anti-phase coupling J(XH), where X = ^{31}P or ^{103}Rh, has been removed. The peaks observed are ECOSY type patterns, where the passive coupling provides the multiplet separation in each dimension. This means that from the ^{1}H–^{31}P correlation, the two couplings $J(^1H,^{103}Rh)$ and $J(^{31}P,^{103}Rh)$ can be measured from the splittings in the ^{1}H and ^{31}P (F2 and F1) dimensions respectively. From the ^{1}H–^{103}Rh correlation the two couplings $J(^1H,^{31}P)$ and $J(^{31}P,^{103}Rh)$ can be measured from the splittings in the F2 and F1 dimensions respectively. In addition to the magnitudes of the couplings, the relative signs of the couplings can be determined from the slope of the lines joining the connected transitions in the multiplet fine structure. If the slope of the line is positive, then the two couplings are of the same sign, and if it is negative they are of opposite sign. From the spectra recorded here for both compounds **5** and **6**, the sign of the coupling $J(P_gH_f)$ is opposite to the sign of the other couplings measured $J(RhH_f)$, $J(RhH_g)$, $J(RhP_g)$, $J(RhP_g)$ and $J(P_fH_f)$.

In the case of the iridium complexes, there are no additional heteronuclear couplings other than those between ^{1}H and ^{31}P present in the spin system. It was therefore not possible to extract the heteronuclear coupling constants between ^{31}P and ^{1}H as passive couplings from heteronuclear Rh–H correlation spectra. Neither was it possible to measure the active couplings between ^{1}H and ^{31}P from the rapidly acquired heteronuclear correlation spectra presented here due to poor digital resolution and rapid relaxation of the products.

Relay experiments

In order to assign resonances for protons that were not directly coupled to the hydride ligands, but also coupled to ^{31}P, magnetisation was relayed across the coupling network $^1H(A) \rightarrow {}^{31}P \rightarrow {}^1H(B)$. Since PHIP enhanced hydride resonances commonly only possess scalar couplings to other hydride ligands, the metal and other metal bound heteronuclei the development of this approach to facilitate the detection of other nuclei was an important requirement. In order to utilise the PHIP hydride enhancement in this way a common heteronuclear coupling partner is required. This method was established using an H–X–H correlation experiment.[21] The only modification made to the sequence was the introduction of an initial π/4 pulse (Fig. 2d). The fixed delays τ_2 and τ_3 both need to be optimised

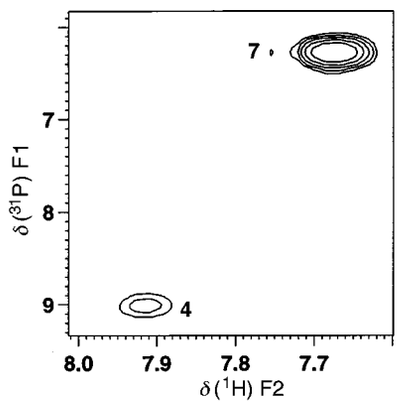

Fig. 7 Inverse relayed $^1H(A)\rightarrow^{31}P\rightarrow^1H(B)$ shift correlation spectrum of the mixture of **4** and **7** formed on addition of *p*-H_2 to **1**, showing cross-peaks (absolute value display) connecting P_a and P_b to their *ortho* phenyl protons (333 K).

experimentally, although in this case, τ_2 had been previously optimised for the HSQC experiments. Using this approach, resonances for the *ortho* phenyl protons of the phosphines in **4** and **7** were enhanced and easily located (Fig. 7). This technique thereby provides a route to the assignment of remote ligand resonances in species that are only detectable because of their *p*-H_2 enhanced proton signature.

Exchange and 3D structure

Dipolar relaxation and the NOESY experiment have been widely utilised to obtain information about internuclear distances and exchange processes.[29] In order for NMR pulse sequences such as NOESY to be applied to systems containing *p*-H_2, it is necessary to refocus the anti-phase magnetisation generated by the initial π/4 pulse using a (τ–π–τ) sandwich, where $\tau = \frac{1}{2}J(H_AH_B)$ (Fig. 2e). The initial anti-phase magnetisation due to the *p*-H_2 enhanced signal ($I_{AZ}I_{BY}$ and $I_{BZ}I_{AY}$) after refocusing (I_{BX} and I_{AX}) follows the usual magnetisation pathways and the remainder of the sequence follows normal methods.

A series of NOESY spectra of the mixture of **4** and **7** were acquired with mixing times (τ_m) ranging between 100 ms and 1.6 s, and total acquisition times between 10 and 20 min. Cross-peaks were only observed as a result of magnetisation transfer from *p*-H_2 enhanced resonances and as a result, the spectra are not symmetrical about the diagonal. Both positive (due to chemical exchange) and negative cross-peaks (due to nOe enhancements) were observed and their intensities increased with mixing time until relaxation effects dominated.

The exchange properties were also found to be highly temperature dependent. At 343 K negative cross-peaks were found to interconnect the hydride ligands of **4**, and also to interconnect the hydride ligands with the *ortho* phenyl protons of the bound phosphine. This experiment thus confirms the validity of the data yielded by the relay approach. In the corresponding NOESY spectrum at 363 K additional positive, or exchange, cross-peaks due to the correlation between the hydride resonances of **7** and those due to free H_2 were observed. Although H_2 exchange at **4** is not evident in the NOESY experiment at 343 K, slow exchange between H_2 and the protons of **4** must be occurring because the hydride resonances of **4** are *p*-H_2 enhanced at this temperature.

Negative cross-peaks were also observed in these experiments between (i) the resonances of H_d and the *ortho* phenyl proton resonances H_h and H_i of P_b and P_c in **7** respectively (relative intensity ≈2:1 reflects their populations, Fig. 8), and (ii) the resonances due to H_c and the *ortho* phenyl protons H_h of P_b (Table 1). These through space interactions confirm that H_c is *trans* to P_c and *cis* to P_b and illustrate that *p*-H_2 enables the rapid probing of the spatial arrangements of ligands around transition metal centres.

Table 1 Percentage cross-peak intensities extracted from NOESY spectra for free H_2 and H_c of **7** relative to the diagonal peak H_d as a function of mixing time (343 K, 45-fold excess of PPh_3 relative to **1**)

Mixing time/ms	Free H_2	H_c	*ortho* phenyl protons of P_b
100	11	13	−4
300	84	72	−19
500	134	76	−53
1600	536	100	−419

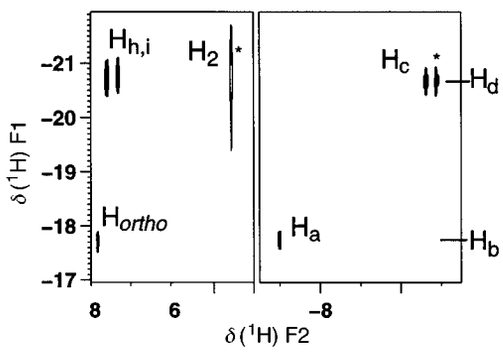

Fig. 8 NOESY spectrum of a mixture of **4** and **7**. The pulse sequence used is given in Fig. 2e. The peaks indicated with * are positive and arise due to exchange while the peaks to H_h and H_i are negative and arise through nOe interaction. Experimental parameters: $\tau_m = 300$ ms, $t_{1max} = 7.9$ ms, $t_{2max} = 56.3$ ms, experimental time = 26 min.

When the related complex $IrCl(AsPh_3)_3$ **9** is examined with *p*-H_2, the corresponding *p*-H_2 enhanced dihydride addition product $Ir(H)_2Cl(AsPh_3)_3$ **10** is detected. The *p*-H_2 enhanced hydride resonances of **10** are located at δ −14.0 and −22.7 with both appearing as simple anti-phase doublets with the phase sense emission/absorption, thereby confirming that *J*(HH) is negative. In the corresponding 2D-NOESY spectrum, collected at 318 K, nOe cross-peaks connect the hydride at δ −22.7 to *ortho* phenyl protons at δ 7.65 and 7.39, and the hydride resonance at δ −14.0 to one *ortho* phenyl proton at δ 7.65. Further cross-peaks connect the hydride resonances to both free H_2 and each other. The latter arise due to nOe and the former due to chemical exchange. This confirms that the resonance at δ −14.0 is *trans* to arsine while that at δ −22.7 is *cis* to two inequivalent arsine ligands. In this case, the NOESY method enables the unambiguous assignment of ligand arrangement and resonance position even though the more usual *trans* and *cis* heteronuclear-hydride couplings are absent.

In the case of complex **7**, cross-peaks due to the exchange between the hydride resonances due to H_c and H_d and the resonance due to free H_2 were observed at 343 K (Fig. 8, Table 1). For a given mixing time, increasing the concentration of free PPh_3 first dramatically increases the intensity of the intramolecular exchange peaks between H_c and H_d, while concurrently reducing intermolecular exchange peaks to free H_2 (Table 2). However, at even higher PPh_3 concentrations (>500-fold excess relative to **1**), the intensity of the self-exchange peaks between H_c and H_d is diminished. In order to ascertain whether P_b and P_c exchange identities, a ^{31}P–^{31}P homonuclear exchange experiment was recorded by initially transferring magnetisation from ^1H to ^{31}P, however, no exchange was observed on the time scale of the experiment.

These results suggest that **7** undergoes exchange of PPh_3 *trans* to hydride to form the 16-electron complex, $IrH_2Cl(PPh_3)_2$ **11** (Scheme 3). Complex **11** can then either recoordinate PPh_3 to reform **7**, or reductively eliminate H_2. The observation that the latter process is suppressed by the addition of PPh_3 is consistent with a reduced lifetime for **11**. Additionally, the observed reduction in the rate of interconversion of H_c and H_d at higher PPh_3 concentrations requires that the hydride ligands of

Table 2 Percentage cross-peak intensities extracted from NOESY spectra for free H_2 and H_c of **7** relative to the diagonal peak H_d as a function of phosphine excess relative to **1** (343 K, mixing time $\tau_m = 100$ ms)

Phosphine excess	Free H_2	H_c
1	33	0.8
45	11	13
149	0	14
408	0	21
556	0	17
708	0	16

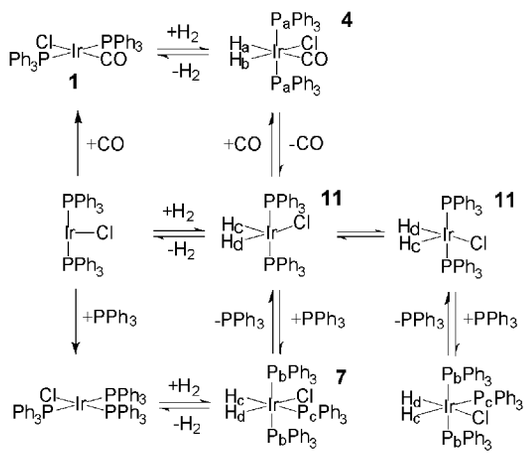

Scheme 3

11 retain a distinct identity (Scheme 3). This suggests that $IrH_2Cl(PPh_3)_2$ must adopt a square-pyramidal geometry in solution with chemically distinct hydrides; the phosphine dependence arises from the step in H_d and H_c exchange identities. This result contrasts with the congener $RhH_2Cl(PPh_3)_2$[30] which has equivalent hydrides and C_{2v} symmetry: $IrH_2Cl(P^tBu_2Ph)_2$, however, has been shown to contain inequivalent hydride ligands.[31]

Experimental time and sensitivity

A significant potential limitation which is a result of using p-H_2 as starting magnetisation is the fact that p-H_2 bound to a metal centre commonly relaxes rapidly and is often only present for a very limited time period (*e.g.* several minutes). However, in an NMR experiment, the recycle time can be very rapid as it is limited by the exchange rate of gaseous H_2 with bound H_2, which can significantly increase the amount of signal obtained in a given period of time. Due to the enhancement of the p-H_2 signal, the sensitivity of the experiments is extremely high and the minimum amount of signal averaging is required. These two factors make it possible to acquire 2D data sets in several minutes. This result is of critical importance because it allows measurement before relaxation causes significant depletion of the p-H_2 spin state population.

Conclusion

The results presented here illustrate the successful application of 2D NMR experiments to monitor p-H_2 enhanced metal hydride complexes. Most 2D experiments can be appropriately modified and applied to p-H_2 enhanced spectra, however only a limited number of experiments are in fact applicable to p-H_2 enhanced spin systems. The heteronuclear correlation experiments make it possible to use the significantly enhanced proton signal to observe heteronuclear signals more readily. This enables the assignment of chemical shifts of lower sensitivity nuclei, in short lived species, and also the measurement of heteronuclear coupling constants which often provide structural information. Furthermore, the NOESY experiments demonstrate that exchange at a relatively slow rate can be observed using p-H_2 due to the significantly enhanced signal intensity.

Two iridium and rhodium phosphine systems which undergo oxidative addition of H_2 have been studied in detail. In the case of $[Rh(PMe_3)_4]Cl$ and $RhCl(PMe_3)_3$ the ^{103}Rh and ^{31}P spectra of the dihydride products were observed using p-H_2 enhancement, and heteronuclear coupling constants were obtained. In the case of $IrCl(CO)(PPh_3)_2$ heteronuclear correlation experiments enabled the assignment of the ^{31}P nuclei in both $IrH_2Cl(PPh_3)_2(CO)$ and $IrH_2Cl(PPh_3)_3$. Furthermore, NOESY experiments are shown to enable the investigation of ligand exchange pathways in p-H_2 products. In the case of $IrH_2Cl(PPh_3)_3$, these studies made it possible to infer that H_2 exchange involves the square-pyramidal intermediate $IrH_2Cl(PPh_3)_2$ with inequivalent hydride ligands. When the NOESY approach was applied to $IrH_2Cl(AsPh_3)_3$ the relative disposition of the ligands about the metal centre was unambiguously determined.

Experimental

All sample preparations were completed in either a nitrogen filled glove box or using a Schlenk line, and solvents were dried and degassed prior to use. NMR samples were run in resealable NMR tubes fitted with J. Young teflon valves, and filled by solvent transfer on a high vacuum line. Triphenylphosphine (Aldrich), trimethylphosphine (Aldrich) and hydrogen (99.99%, BOC) were used as received. $IrCl(CO)(PPh_3)_2$ **1**, $[Rh(PMe_3)_4]Cl$ **2**, $RhCl(PMe_3)_3$ **3**, and $IrCl(AsPh_3)_3$ **9**, were prepared according to literature methods.[32]

For the PHIP experiments, hydrogen enriched in the *para* spin state was prepared by cooling H_2 to 77 K over a paramagnetic catalyst as described previously.[4] Three atmospheres of H_2 were added to the resealable NMR tube on a high vacuum line. The samples were thawed immediately prior to use and introduced into the NMR spectrometer at a preselected temperature. p-H_2 enhanced NMR spectra were recorded on Bruker AMX-500 and DRX-400 spectrometers (York) with ^1H at 500.13 and 400.13, ^{31}P at 202.46 and 161.98, and ^{103}Rh at 15.737 MHz. ^1H NMR chemical shifts are reported in ppm relative to residual ^1H signals in the deuteriated solvents (benzene-d_6 $\delta = 7.13$ and toluene-d_8 $\delta = 2.13$, methylenechloride-d_2 $\delta = 5.26$). ^{31}P-{^1H} NMR spectra are reported in ppm downfield of an external 85% solution of phosphoric acid and ^{103}Rh spectra are reported relative to 3.16 MHz $\delta = 0$.

In all cases, 1D ^1H spectra were first recorded in order to measure the value of J(X-H) used for multiplet selection in the 2D sequence and to optimise the temperature for a given experiment time. For example, at 343 K in benzene-d_6 the hydrides of **7** briefly show 200-fold enhancement. However, at 312 K, in methylenechloride-d_2 the initial hydride signal enhancement falls to 30-fold but remains appreciable for up to 20 min. In addition, we independently optimised the recycle time to yield the maximum refreshed signal for each sample/temperature (typically this lies between 20 and 100 ms) and between 1024 and 256 increments are recorded. Only increments stored before the p-H_2 enhancement drops to zero (no signal) are used in the transformed data. Phase-sensitive acquisition was achieved using TPPI (time proportional phase incrementation)[33] by incrementing the phase of the first pulse to the heteronucleus (X) by $\pi/2$ for each slice of the 2D data set.

Spectroscopic data for **4** and **7** in toluene-d_8, **5** and **6** in methylenechloride-d_2, and **10** in benzene-d_6. **4**: ^1H (343 K) δ 7.91 {*ortho* phenyl proton attached to P_a}, −7.02 {H_a, $J(P_aH) = 18.8$, $J(HH) = -5.7$}, −17.6 {H_b, $J(PaH) = 13.7$, $J(HH) = -5.7$ Hz}; ^{31}P (343 K) δ 8.4 {P_a, s}. **5**: ^1H (300 K) δ −10.72 {2H, m, $J(P_eH_{trans}) = 139$, $J(P_eH_{cis}) = 32.7$, $J(RhH) = 14.5$, $J(P_dH) = 20.3$ Hz}; ^{31}P (300 K) δ −12.6 {P_d, dt,

$J(P_dRh) = 96$, $J(P_dP_e) = 28$}, −23.6 {P_e, dt, $J(P_eRh) = 86$, $J(P_dP_e) = 28$ Hz); ^{103}Rh (312 K) δ −1007 {tt, $J(P_eRh) = 86$, $J(P_dRh) = 96$ Hz}. **6**: ^{1}H (312 K) δ −9.79 {H_f, $J(P_fH) = 176$, $J(P_gH) = -19$, $J(RhH) = 15$, $J(HH) = -8$}, −19.5 {H_g, $J(RhH) = 27$, $J(P_fH) = 13$, $J(P_gH) = 20$, $J(HH) = -8$ Hz}; ^{31}P (312 K) δ −7.4 {P_g, dd, $J(P_gRh) = 103$, $J(PP) = 28$}, −21.3 {P_f, dt, $J(P_fRh) = 88$, $J(PP) = 28$ Hz}; ^{103}Rh (312 K) δ −319 {dt, $J(PRh) = 88$, $J(PRh) = 103$ Hz}. **7**: ^{1}H (343 K) δ 7.67 {H_h, *ortho* phenyl proton attached to P_b}, 7.42 {H_i, *ortho* phenyl proton attached to P_c}, −10.8 {H_c, $J(P_bH) = 20.6$, $J(P_cH) = 130.6$, $J(HH) = -7$}, −20.6 {H_d, $J(P_bH) = 14.3$, $J(P_cH) = 14.3$, $J(HH) = -7$ Hz}; ^{31}P (343 K) δ −2.8 {P_c, t, $J(PP) = 26$}, 5.7 {P_b, d, $J(PP) = 26$ Hz}. **10**: ^{1}H (318 K) δ 7.65 {H_m, *ortho* phenyl proton attached to As_a}, 7.39 {H_n, *ortho* phenyl proton attached to As_b}, −22.7 {H_l, $J(H_lH_k) = -5.7$}, −14.0 {H_k, $J(H_kH_l) = -5.7$ Hz}.

Acknowledgements

We are grateful to the University of York (M. G. P.) and the Royal Society (field gradient unit and a study visit grant for Australia to S. B. D.), the SCI, the EPSRC (C. J. S. and spectrometer), Bruker UK (spectrometer), NATO, and the Australian Research Council (B. A. M.) for financial support. A generous loan of iridium and rhodium trichloride from Johnson Matthey is acknowledged. We appreciated helpful discussions with Professor R. Eisenberg, Professor L. D. Field, Dr G. K. Barlow and Dr J. A. B. Lohman.

References

1 J. Natterer and J. Bargon, *Prog. Nucl. Magn. Reson. Spectrosc.*, 1997, **31**, 293.
2 C. R. Bowers and D. P. Weitekamp, *Phys. Rev. Lett.*, 1986, **57**, 2645.
3 C. R. Bowers and D. P. Weitekamp, *J. Am. Chem. Soc.*, 1987, **109**, 5541.
4 R. Eisenberg, *Acc. Chem. Res.*, 1991, **24**, 110.
5 J. Barkemeyer, M. Haake and J. Bargon, *J. Am. Chem. Soc.*, 1995, **117**, 2927.
6 M. Jang, S. B. Duckett and R. Eisenberg, *Organometallics*, 1996, **15**, 2863.
7 S. B. Duckett and R. Eisenberg, *J. Am. Chem. Soc.*, 1993, **115**, 5292.
8 S. B. Duckett, C. L. Newell and R. Eisenberg, *J. Am. Chem. Soc.*, 1994, **116**, 10548.
9 See for example, J. Barkemeyer, M. Haake and J. Bargon, *J. Am. Chem. Soc.*, 1995, **117**, 2927.
10 C. J. Sleigh and S. B. Duckett, *Prog. Nucl. Magn. Reson. Spectrosc.*, 1999, **34**, 71.
11 S. B. Duckett, R. J. Mawby and M. G. Partridge, *Chem. Commun.*, 1996, 383.
12 C. J. Sleigh, S. B. Duckett and B. A. Messerle, *Chem. Commun.*, 1996, 2395.
13 S. B. Duckett, G. K. Barlow, M. G. Partridge and B. A. Messerle, *J. Chem. Soc.*, *Dalton Trans.*, 1995, 3427.
14 O. W. Sorensen, G. W. Eich, M. H. Levitt, G. Bodenhausen and R. R. Ernst, *Prog. Nucl. Magn. Reson. Spectrosc.*, 1983, **16**, 163.
15 C. R. Bowers, D. P. Weitekamp, *Phys. Rev. Lett.*, 1986, **57**, 2645.
16 L. Vaska, *Acc. Chem. Res.*, 1968, **1**, 355.
17 R. R. Schrock and J. A. Osborn, *J. Am. Chem. Soc.*, 1971, **93**, 2397.
18 R. A. Jones, F. M. Real, G. Wilkinson, A. M. R. Galas, M. B. Hursthouse and K. M. A. Malik, *J. Chem. Soc.*, *Dalton Trans.*, 1980, 511.
19 G. M. Intille, *Inorg. Chem.*, 1972, **11**, 695.
20 W. P. Aue and E. Bartholdi and R. R. Ernst, *J. Chem. Phys.*, 1976, **64**, 2229; K. Nagayama, A. Kumar, K. Wüthrich and R. R. Ernst, *J. Magn. Reson.*, 1980, **40**, 321.
21 G. Bodenhausen and D. J. Ruben, *J. Chem. Phys. Lett.*, 1980, **69**, 185.
22 G. A. Morris and R. Freeman, *J. Am. Chem. Soc.*, 1979, **101**, 760.
23 A. Bax, R. H. Griffey and B. L. Hawkins, *J. Magn. Reson.*, 1983, **55**, 301.
24 P. Güntert, W. Braun, M. Billeter and K. Wüthrich, *J. Am. Chem. Soc.*, 1989**,** **111**, 3997; M. Karplus, *J. Am. Chem. Soc.*, 1963, **85**, 2870; V. F. Bystrov, *Prog. NMR Spectrosc.*, 1976, **10**, 41.
25 D. S. Moore and S. D. Robinson, *Chem. Soc. Rev.*, 1983, **12**, 415; H. D. Kaesz and R. B. Saillant, *Chem. Rev.*, 1972, **72**, 231; N. Bampos, L. D. Field and B. A. Messerle, *Organometallics*, 1993, **12**, 2529.
26 C. Griesinger, O. W. Sorensen and R. R. Ernst, *J. Am. Chem. Soc.*, 1985, **107**, 6394; C. Griesinger, O. W. Sorensen and R. R. Ernst, *J. Chem. Phys.*, 1986, **85**, 6837.
27 L. Emsley and G. Bodenhausen, *J. Am. Chem. Soc.*, 1991, **113**, 3309; H. Kessler, S. Mronga and G. Gemmecker, *Magn. Reson. Chem.*, 1991, **29**, 527.
28 G. Otting, B. A. Messerle and L. P. Soler, *J. Amer. Chem. Soc.*, 1997, **119**, 5425, and refs. therein.
29 H. Kessler, M. Gehrke and C. Griesinger, *Angew. Chem.*, *Int. Ed. Engl.*, 1988, **27**, 490; D. Neuhaus and M. P. Williamson, *The Nuclear Overhauser Effect in Structural and Conformational Analysis*, VCH Publishers, Weinheim, 1989; R. R. Ernst, G. Bodenhausen and A. Wokaun, *Principles of Nuclear Magnetic Resonance in One and Two Dimensions*, Oxford University Press, 1987.
30 J. M. Brown, P. L. Evans and A. R. Lucy, *J. Chem. Soc.*, *Perkin Trans 2.*, 1987, 1589.
31 B. E. Hauger, D. Gusev and K. G. Caulton, *J. Am. Chem. Soc.*, 1994, **116.** 208; A. Albinati, V. I. Bakhmutov, K. G. Caulton, E. Clot, J. Eckert, O. Eisenstein, D. G. Gusev, V. V. Grushin, B. E. Hauger, W. Klooster, T. F. Koetzle, R. K. McMullan, T. L. O'Loughlin, M. Pelissier, J. S. Ricci, M. P. Signalas and A. E. Vymenits, *J. Am. Chem. Soc.*, 1993, **115**, 7300.
32 J. P. Collman, C. T. Sears, Jr. and M. Kubota, *Inorg. Synth.* 1968, **11**, 101; R. A. Jones, F. M. Reed, G. Wilkinson, A. M. R. Galas, M. B. Hursthouse and K. M. A. Malik, *J. Chem. Soc.*, *Dalton Trans.*, 1980, 511.
33 D. Marion and K. Wüthrich, *Biochem. Biophys. Res. Commun.*, 1983, **113**, 967; A. G. Redfield and S. D. Kunz, *J. Magn. Reson.*, 1975, **19**, 250.

Paper 8/09948K